Self-consistent heavy-ion potentials*

P. G. Zint and U. Mosel
Institut für Theoretische Physik, Universität Giessen 63 Giessen, West Germany
(Received 18 June 1976)

Calculations of the real part of the heavy-ion potential have been performed for the systems $^{12}C + ^{12}C$, $^{16}O + ^{16}O$, and $^{40}Ca + ^{40}Ca$ using the Hartree-Fock method with a constraint on the center-of-mass distance. The interaction used is the Skyrme force SIII. For the case of $^{16}O + ^{16}O$ a detailed discussion of the nuclear structure with increasing overlap of the ions is given. It is found that the individual shell structures of the two ^{16}O nuclei survive until the density in the neck region has reached about 50% of its maximum value. The calculated potentials have been used in an optical model code to calculate elastic excitation functions. The agreement with the empirically determined best fit potentials is remarkable.

[NUCLEAR REACTIONS Self-consistent constrained Hartree-Fock calculations of HI potentials. Structure of $^{16}O + ^{16}O$ at large overlap; potentials calculated for $^{12}C + ^{12}C$, $^{16}O + ^{16}O$, $^{40}Ca + ^{40}Ca$; compared with experimental fits.]

I. INTRODUCTION

One of the main problems in heavy-ion (HI) physics is the determination of the optical potential for heavy ions. Whereas for the imaginary part only very few calculations exist so far,[1,2] many attempts have been made to calculate the real part of the optical potential.[3-13] Because of its simplicity one of the most popular approaches has been to use the folding method.[14-17] However, that version of the folding method that uses nucleon-nucleon potentials *empirically* determined from α-particle scattering can obviously not easily be extrapolated to heavy-ion systems. If, on the other hand, one starts with a free nucleon-nucleon force then many of these forces yield HI potentials that are too deep at the strong absorption radius.[14] Satchler[14] has hinted that this effect could be due to the neglect of dynamical or static distortions of the nuclear density distributions as the nuclei come into contact.

On the other hand it has been shown that the Pauli principle plays an important role in HI potentials even at small overlaps. This is not taken into account in the folding procedure.[18] It was, therefore, our aim to determine the real part of the potential in a method that is free of this shortcoming. To this purpose we have performed Hartree-Fock (HF) calculations with the distance between the centers of mass of the two ions as a constraint. The Skyrme force was used as an effective interaction. The energy curve as a function of the distance was then interpreted as the real optical potential. The underlying concept for this procedure is the Born-Oppenheimer approximation. In Sec. II we present a detailed description of our method and apply it to the investigation of the structure of the $^{16}O + ^{16}O$ system in Sec. III.

II. TWO-CENTER HARTREE-FOCK METHOD

The extensive application of the Skyrme force by Vautherin and Brink[19] and Flocard *et al.*[20] to nuclear ground state properties has opened up new possibilities in a theoretical treatment of nuclei. The main advantage of this type of force in HF calculations is the fact that the total energy E of the system can be written as a functional of a few densities and that the resulting HF equations are partial differential equations. Presently we restrict our investigations to systems with axial symmetry consisting of two identical nuclei, which have an even number of protons and neutrons. As reported earlier[21] we solve the HF equations in the basis of the eigenfunctions of the two-center harmonic oscillator.[22] With these basis functions one can describe in a natural way the various nuclear shapes from very small deformations to even separated systems. It should be noted explicitly that for center distance zero this basis agrees with the usual deformed harmonic oscillator basis.

The degree of deformation in our model is fixed by the expectation value of the operator

$$\hat{r} = \frac{2}{A} \sum_{i=1}^{A} |z_i| \tag{1}$$

for the distance between the centers of mass (c.m.) of the interacting nuclei with mass number $A/2$. Here z is the coordinate of the symmetry axis, i.e. the axis through the two centers of mass, with its origin in the middle of the two centers. This distance is fixed in our HF calculations by means of a quadratic constraint

$$F = \tfrac{1}{2} p (r - r_0)^2 \tag{2}$$

in order to obtain all points of the curve $E(r)$. The quantity p is a fixed coupling parameter and r_0 is a variable which can be used to force the system into various deformations $r=\langle\hat{r}\rangle$. With this constraint one has to solve the following set of constrained HF (CHF) equations:

$$H^{q_K}_{\mathrm{CHF}}\Phi_K=\left[-\vec{\nabla}\left(\frac{\hbar^2}{2m^*_{q_K}}\vec{\nabla}\right)+U_{q_K}-i\vec{W}_{q_K}\cdot\vec{\nabla}\times\vec{\sigma}\right]\Phi_K=\epsilon_K\Phi_K \tag{3}$$

with

$$\frac{\hbar^2}{2m^*_{q_K}}=\frac{\hbar^2}{2m}+\tfrac{1}{4}(t_1+t_2)\rho+\tfrac{1}{8}(t_2-t_1)\rho_{q_K}, \tag{4}$$

$$\begin{aligned}U_{q_K}=t_0[(1+\tfrac{1}{2}x_0)\rho-(x_0+\tfrac{1}{2})\rho_{q_K}]+\tfrac{1}{8}(t_2-3t_1)\Delta\rho+\tfrac{1}{16}(3t_1+t_2)\Delta\rho_{q_K}+\tfrac{1}{4}(t_1+t_2)\tau+\tfrac{1}{8}(t_2-t_1)\tau_{q_K}\\+\tfrac{1}{4}t_3(\rho^2-\rho_{q_K}{}^2)-\tfrac{1}{2}W_0(\vec{\nabla}\vec{J}+\vec{\nabla}\vec{J}_{q_K})+\delta_{q_K,p}[V_C-e_0{}^2(3/\pi)^{1/3}\rho_p{}^{1/3}]+p(r-r_0)2/A\,|z_K|,\end{aligned} \tag{5}$$

$$\vec{W}_{q_K}=\tfrac{1}{2}W_0(\vec{\nabla}\rho+\vec{\nabla}\rho_{q_K})+\tfrac{1}{8}(t_1-t_2)\vec{J}_{q_K} \tag{6}$$

and the densities

$$\rho_{q_K}=\sum_m|\Phi_m|^2, \tag{7}$$

$$\tau_{q_K}=\sum_m|\vec{\nabla}\Phi_m|^2, \tag{8}$$

$$\vec{J}_{q_K}=-i\sum_m\Phi^*_m[\vec{\nabla}\Phi_m\times\vec{\sigma}] \tag{9}$$

written in a condensed way. The Coulomb exchange potential is treated in the Thomas-Fermi approximation.

Here $\vec{\sigma}$ indicates the spin operator. V_C is the direct term of the Coulomb interaction. The quantities t_0, t_1, t_2, t_3, x_0, and W_0 are the Skyrme parameters. All calculations reported in this paper are done with the set Skyrme III.[20] As mentioned above, we expand the eigenfunctions Φ_K which are classified by the component of the angular momentum in z direction Ω, the parity π, and a third quantum number n:

$$\begin{aligned}&\Phi_K=\sum_j c^K_j\psi_j,\quad K=(\Omega,\pi,n),\quad j=(n_\phi,n_r,n_z),\\&\psi_j=\frac{1}{\sqrt{2\pi}}e^{in_\phi\cdot\phi}N^{|n_\phi|}_{n_r}\sqrt{K_r}\,e^{-\rho/2}\rho^{|n_\phi|/2}L^{|n_\phi|}_{n_r}(\rho)N_{n_z}\\&\quad\times4\sqrt{K_z}D_{n_z}(\sqrt{2}\,\xi)P,\\&K_r=\frac{m\omega_r}{\hbar},\quad K_z=\frac{m\omega_z}{\hbar},\quad\rho=K_r(x^2+y^2),\\&\xi=\sqrt{K_z}(|z|-z_0),\quad N^{n_\phi}_{n_r}=\left(\frac{2n_r!}{(n_r+n_\phi)!}\right)^{1/2},\\&N_{n_z}=\left[\sqrt{2}\int_{-\sqrt{2K_z}z_0}^{\infty}D_{n_z}{}^2(t)dt\right]^{-1/2},\\&P=\begin{cases}-1 & \text{for } z<0 \text{ and negative } z \text{ parity}\\ 1 & \text{otherwise}\end{cases}\end{aligned} \tag{10}$$

ω_r and ω_z are the oscillator parameters of the two-center oscillator. z_0 is its distance parameter. $L^{n_\phi}_{n_r}$ are the Laguerre polynomials and $D_{n_z}(z)$ is the parabolic cylinder function[23]:

$$D_{n_z}(z)=e^{-z^2/4}\sum_K\binom{n_z}{K}z^K\sqrt{\pi}\times\{2^{-(n_z-K)/2}\Gamma[-\tfrac{1}{2}(n_z-K)+\tfrac{1}{2}]\}^{-1}. \tag{11}$$

For large values of z and small n_z there is a semi-convergent expansion for $D_{n_z}(z)$:

$$\begin{aligned}&D_{n_z}(z)=z^{n_z}e^{-z^2/4}\left[\sum_{n=0}^{N}c_n+O(|z^2|^{-N-1})\right],\quad z\gg1,\\&D_{n_z}(z)=z^{n_z}e^{-z^2/4}\left[\sum_{n=0}^{N}c_n+O(|z^2|^{-N-1})\right]\\&\quad-\sqrt{2\pi}\,\Gamma^{-1}(-n_z)\frac{1}{z}\left[\sum_{n=0}^{N}d_n+O(|z^2|^{-N-1})\right]\\&\quad\times|z|^{-n_z}e^{z^2/4},\qquad z\ll-1\end{aligned} \tag{12}$$

with the abbreviations

$$\begin{aligned}&c_n=[(-\tfrac{1}{2}n_z)_n(-\tfrac{1}{2}n_z+\tfrac{1}{2})_n]/\{n![\tfrac{1}{2}(-z^2)]^n\},\\&d_n=[(\tfrac{1}{2}n_z+\tfrac{1}{2})_n(\tfrac{1}{2}n_z+\tfrac{2}{2})_n]/[n!(\tfrac{1}{2}z^2)^n],\\&(a)_n=a(a+1)\cdots(a+n-1),\quad(a)_0=1.\end{aligned}$$

Since Ω and π are good quantum numbers one only has to diagonalize submatrices with fixed (Ω,π).

The self-consistent calculations are performed as usual in an iteration procedure. Initial guesses for the densities ρ and τ are obtained either from the lowest two-center oscillator wave functions or through the diagonalization of a deformed Woods-Saxon type potential. For computational efficiency the values of the basis functions at given mesh points $(IJ)\equiv(\rho_I,\xi_J)$ are calculated only once initially and then stored. From these the densities are

calculated by summing the single particle densities in r space instead of using the density matrix as described by Vautherin.[24]

The location of the mesh points is determined by the integration formula used for the calculation of the HF Hamiltonian matrix. In the ρ direction we use an 8 point Gauss-Laguerre and in the ξ direction a 16 point Gauss integration formula. In this latter case a finite interval formula was found to yield more accurate results than a Gauss-Hermite formula.

From the initial guesses for ρ, τ, and $\vec{J}$ one calculates the effective mass $m_q^*(IJ)$ and the potentials $U_q(IJ)$ and $\vec{W}_q(IJ)$ that determine the HF matrix. After diagonalization its eigenfunctions can be used to calculate new potentials for a repetition of the iteration procedure. We have found that an averaging over results of consecutive iterations considerably improves the convergence.

Since in practical calculations the basis size is limited, the HF result depends on the basis parameters ω_r, ω_z, and z_0. Therefore, one has to vary these quantities in order to obtain the lowest possible energy. This procedure, however, leads to a difficulty: The constraint parameter r_0 is fixed when one varies the basis parameters. For each set of $(\omega_r, \omega_z, z_0)$ one obtains different values for the energy E and the expectation value r. If one plots each pair (r, E) in a diagram, the resulting lower envelope of these points supplies the desired curve $E(r)$.

In order to obtain the total intrinsic energy of the system we subtract the kinetic energy of the total A-particle system. A completely correct treatment of the operator

$$\frac{1}{2mA}\left(\sum_{i=1}^{A}\vec{p}_i\right)^2$$

in the framework of Skyrme HF calculations is quite tedious. We, therefore, subtract the direct term only which can be done by replacing $\hbar^2/2m$ by $\hbar^2/2m\,(1-1/A)$.

In the Born-Oppenheimer approximation we now identify the difference $E(r)-E(\infty)$ as the real part of the potential $U(r)$. It has to be pointed out that the question of treating the remaining energy of the relative motion is still open. For a discussion of this problem see e.g., Refs. 11, 21, and 25. As will be shown later, we give results only in the region of relatively large r. There the redundant relative energy is nearly constant and can be neglected [see Fig. 2(b) in Ref. 11].

III. STRUCTURE OF THE ^{16}O + ^{16}O SYSTEM

Before presenting the potentials for the various scattering problems we discuss our results for the system consisting of two ^{16}O clusters. Both substructures have magic character. Therefore, it is interesting to study the breakup of these stable shell structures when the nuclei come into contact. Furthermore, the ^{16}O + ^{16}O scattering data require an exact knowledge of the potential even at distances smaller than for neighboring systems. Finally, the compound system ^{32}S has a prolate ground state deformation. A good description should provide this deformation. First results on these points have already been published elsewhere[21] (see also Ref. 26).

As a basis we have used the lowest 44 two-center oscillator wave functions, which corresponds to 4 oscillator shells for each of the ^{16}O nuclei in the limit of large separations. In Fig. 1 we present the single particle spectrum for protons (for the neutron spectrum see Fig. 1 in Ref. 21). The single particle energies are plotted as a function of the separation distance r of the c.m. of the ^{16}O clusters. It should be noted that because of the definition (1) the point $r=3$ fm corresponds to the spherical configuration of the compound system. Here one recognizes the usual degeneracy of the spherical single particle levels. They are classified by the quantum numbers of the spherical oscillator. The region of large r values corresponds to the case of two well separated ^{16}O nuclei. Here

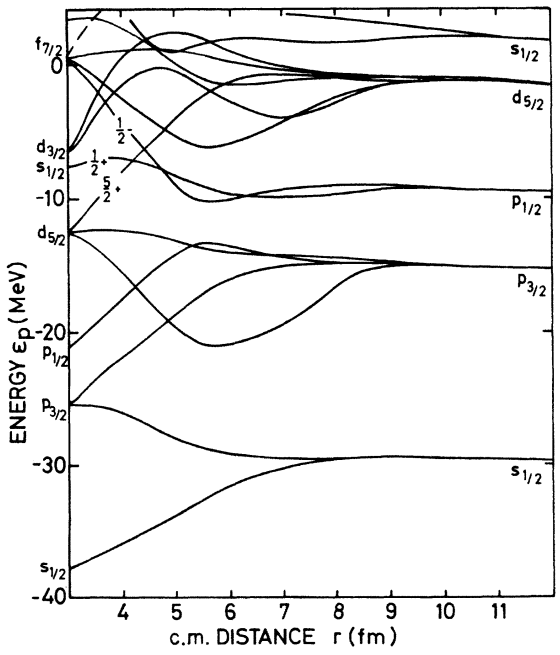

FIG. 1. Single particle energies of protons for the system ^{16}O + ^{16}O as a function of the c.m. distance r. The asymptotic spherical shells are characterized by their quantum numbers. For three single particle states also $(\Omega\pi)$ is given.

again one can use the classification of the spherical oscillator. In the region between these two limiting cases only the quantum numbers Ω and π can be used to classify the states. The proton spectrum has qualitatively the same structure as the neutron spectrum (see Ref. 21). The Coulomb force pushes the levels up and changes the shapes of the energy curves somewhat.

The shells of the magic ^{16}O nuclei dissolve in the region of large density overlap (i.e., small r). For distances $r \gtrsim 4.5$ fm, however, they remain remarkably intact. One sees from Fig. 1 that even though there the Ω degeneracy of the single particle states is broken, the occupied states still have the same structure as at $r \to \infty$. In particular, the highest occupied states are $(\Omega\pi) = (\frac{1}{2}-)$ and $(\frac{1}{2}+)$ states originating in the fragment $p_{1/2}$ shell. This means that the density distribution of the ^{16}O nuclei is somewhat distorted but not destroyed. At $r \approx 4.5$ fm this situation, however, changes: A $(\frac{5}{2}+)$ state of the $d_{5/2}$ shell dives down through the Fermi surface and crosses a $(\frac{1}{2}-)$ state of the $p_{1/2}$ shell of the spherical ^{32}S configuration. At this point, therefore, the density is changed considerably; matter is moved from the z into the ρ direction, thus filling in the neck.

In Fig. 2 the curve $E(r)$ represents the intrinsic energy of the system after removing the energy of the center-of-mass motion of the total system and the spurious energy of the relative motion of the two ^{16}O fragments. The latter energy is calculated according to an interpolation formula

$$T_{sp}(r) = T_{sp}(\infty)\frac{T(r) - T(^{32}\mathrm{S})}{T(\infty) - T(^{32}\mathrm{S})} , \qquad (13)$$

where $T(r)$ is the total kinetic energy as obtained in the HF calculations and $T_{sp}(\infty)$ is the spurious energy for infinite distance. A motivation for this formula can be given by means of a cluster model analysis of the $\alpha + \alpha \to {}^{8}$Be system.[25] The value of T_{sp} is similar to that obtained in Ref. 11 on the basis of a generator-coordinate consideration.

For large r values $E(r)$ exhibits a barrier whose maximum is located at 8.4 fm. The barrier height relative to the value at infinity is in good agreement with the experimental data of Maher *et al.*[31] The absolute minimum of the curve which is interpreted as the ground state of ^{32}S lies at $r = 3.5$ fm. This corresponds to a proton quadrupole moment $Q_p = 45$ fm^2, which has to be compared with an experimental charge quadrupole moment $Q_c = 47$ fm^2. The difference in binding energy for the ground state of $B_{CHF} = 265$ MeV and $B_{exp} = 271$ MeV can be improved by increasing the basis and by projecting to good angular momentum. In the present context we are interested only in the interaction potential, i.e. the value of $E(r)$ *relative* to its value at

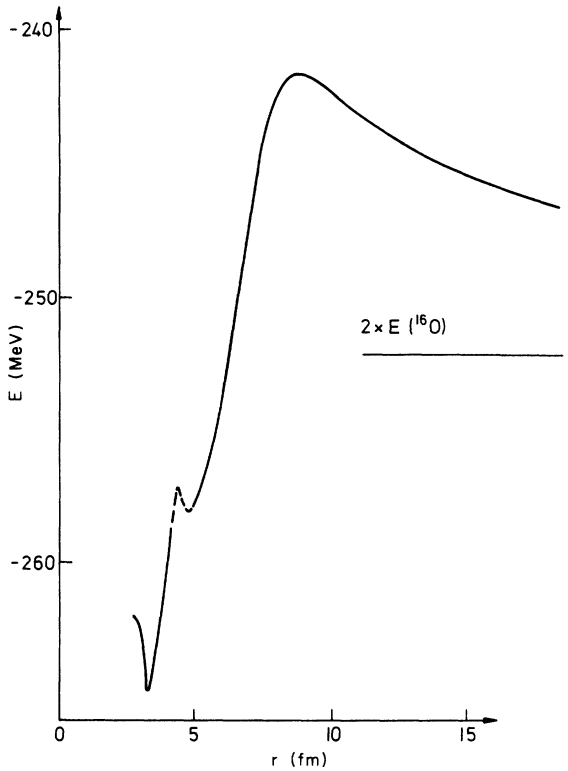

FIG. 2. Total intrinsic energy of the ^{16}O + ^{16}O system as a function of the c.m. distance r. The height of the inner barrier at $r \approx 5$ fm is sensitive to the exact pairing strength and, therefore, somewhat uncertain.

$r \to \infty$. Therefore, the potential should be much more reliable than the difference between the theoretical and the experimental binding energies might otherwise suggest.

Another interesting feature of Fig. 2 is the occurrence of a second minimum at $r = 4.9$ fm besides the ground state minimum. The corresponding value for the proton quadrupole moment is $Q_p = 195$ fm^2. Krieger and Wong obtained a quite similar result using a Nestor two body potential[27] in a CHF calculation. They obtained two minima at mass quadrupole moments $Q = 102$ fm^2 (ground state) and $Q = 340$ fm^2. The relative height between the two extrema was 4 MeV whereas our result is of the order of the value in the liquid drop model (8–9 MeV). The existence of the second minimum can be understood in terms of the single particle spectrum. Stretching the ^{32}S nucleus the energy increases due to the $(\frac{5}{2}+)$ state which rises strongly with r. At $r = 4.5$ fm the quantum numbers of the highest occupied level change and a lower energy is obtained if the last particles fill the $(\frac{1}{2}-)$ state. At this point, therefore, the energy drops down somewhat. At still larger r the rise in energy continues creating the second minimum.

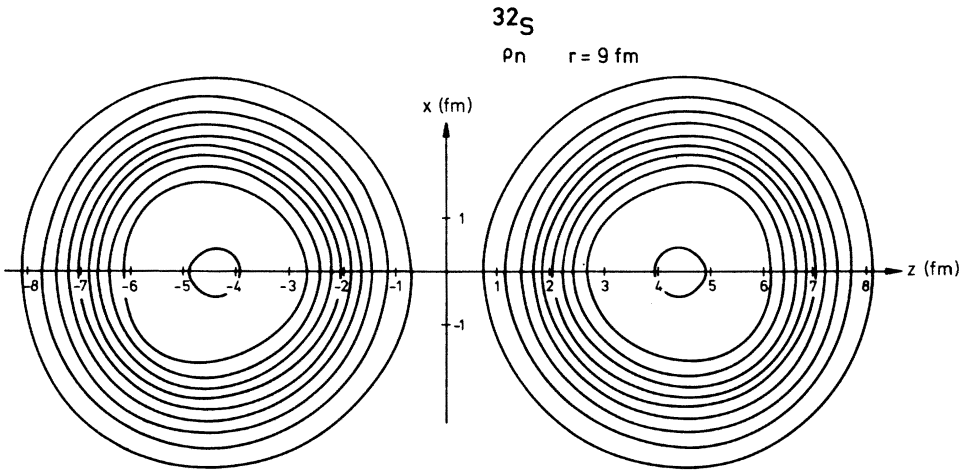

FIG. 3. Contour plot of the neutron density of $^{16}O+^{16}O$ at a c.m. distance of 9 fm. The contour lines are drawn in steps of 10% of the central density from 10 to 90%.

Vershinin and Cherdantsev[28] have studied the influence of an additional minimum in the potential on the scattering cross sections. They found that this minimum can cause intermediate structure in the excitation functions. The experimental data show such structure in the elastic scattering cross sections of the $^{16}O+^{16}O$ scattering. Therefore, the intermediate structure of the excitation function could have its origin in the level crossings of the single particle states of the oxygen systems. However, it remains to be seen whether inclusion of an imaginary potential in the calculation of the excitation functions would not smooth out and thus destroy any intermediate stucture.

In order to study the structure of the $^{16}O+^{16}O$ system we now present some density distributions. With their help one can obtain information on when the shell structure of the two ^{16}O nuclei is dissolved and the ^{32}S cluster becomes dominant. For this purpose, we show contour plots of the neutron density for various values of the distance r. The lines represent curves of 10%, 20%, ..., 90% of the central density. The symmetry axis is given by z; x denotes a coordinate perpendicular to this axis. We start with a plot at $r=9$ fm, i.e., just outside the interaction barrier (Fig. 3). The ^{16}O clusters are separated. But one recognizes a small polarization of the oxygen systems since the density lines are no longer circles. The next plot in Fig. 4 gives the density just inside the barrier at $r=8.3$ fm. The deformation of the ^{16}O clusters has increased; the 10% line is connected. In Fig. 5 the density at the second minimum ($r\sim4.9$ fm) is shown. The shape of the nuclei has changed dras-

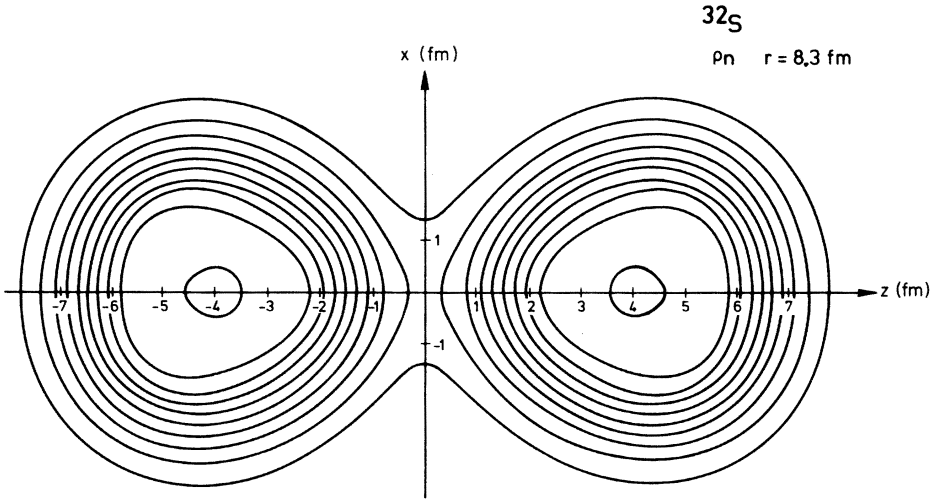

FIG. 4. Neutron density contour plot of $^{16}O+^{16}O$ at a c.m. distance of 8.3 fm.

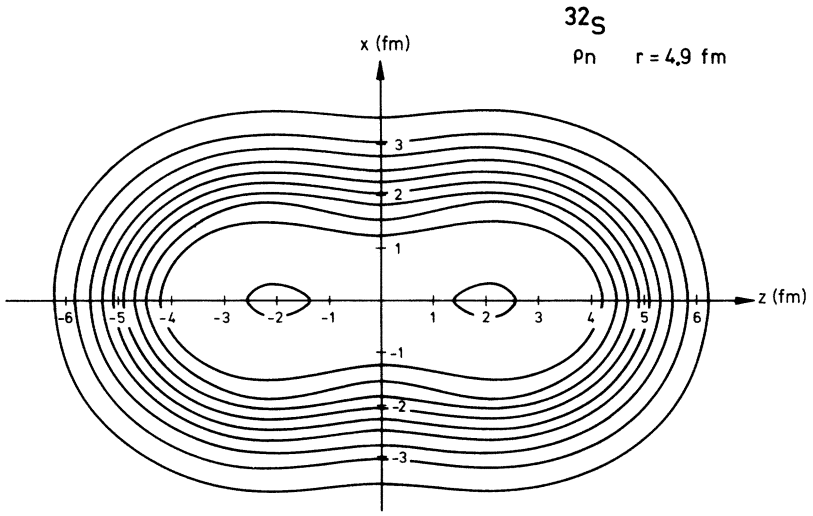

FIG. 5. Neutron density contour plot of $^{16}O+^{16}O$ at a c.m. distance of 4.9 fm (second minimum).

tically. But there is still a two-center structure. Finally we present in Fig. 6 the contour plot for the ground state minimum. Now the dominant maximum of density is located at the center of the system. The oxygen structures are completely washed out. The density is determined by the shells of the compound system.

In the last part of this section we compare the self-consistently calculated direct term of the Coulomb energy E_C^d with the energy of two point charges V_C and that of a point charge in an extended charge distribution (dot-dashed curve in Fig. 7) as usually used in optical model codes. In Fig. 7 we show these quantities as a function of the separation distance. The difference between all curves is very small in the region $r \gtrsim 5.5$ fm of the order of 100 keV. One may conclude that the finite size effect with regard to the Coulomb energy is not large and can be neglected. This result is in agreement with an earlier, more phenomenological study of this point.[29] It has also been noted in Refs. 30 and 31 that even larger discrepancies in the Coulomb potential in the overlap region would be masked by the absorptive part of the potential.

IV. POTENTIALS AND EXCITATION FUNCTIONS

In this section we present the self-consistently calculated potentials $U(r)$ together with excitation functions calculated from them in an optical model

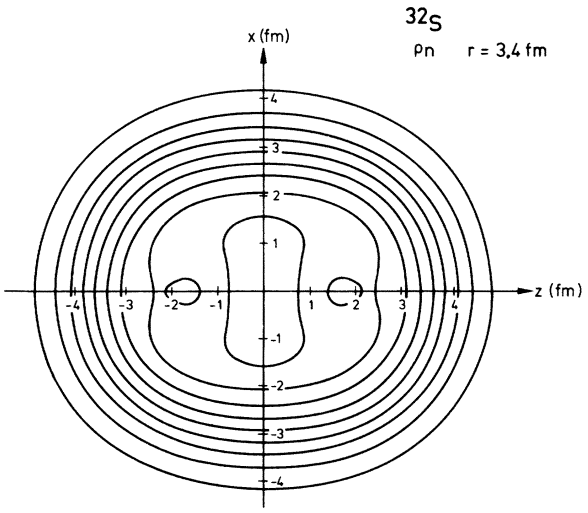

FIG. 6. Neutron density contour plot of the ground state of ^{32}S.

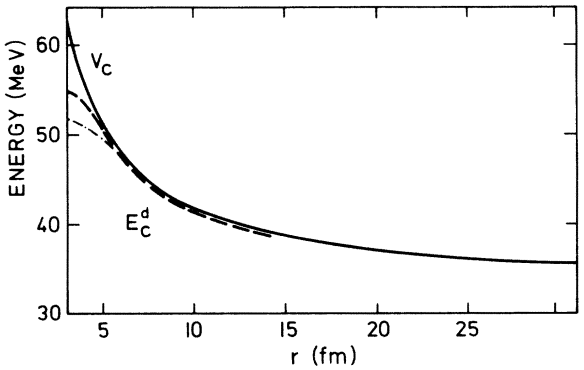

FIG. 7. Coulomb energy E_C^d of the extended $^{16}O+^{16}O$ system compared with the Coulomb energy V_C of two point charges and the potential of a point charge in the field of an extended distribution (dot-dashed) as usually used in optical model calculations as a function of the c.m. distance r.

TABLE I. Woods-Saxon parameters of empirically determined (exp) and calculated (CHF) potentials.

	$^{12}C+^{12}C$		$^{16}O+^{16}O$		$^{40}Ca+^{40}Ca$	
	Exp.[a]	CHF	Exp.[b]	CHF	Exp.[c]	CHF
V_0 (MeV)	14	14	17	19	25	25
R (fm)	6.13	6.13	6.8	6.69	9.23	8.94
a (fm)	0.49	0.56	0.49	0.56	0.49	0.58
W (MeV)	$0.4+0.14E_{c.m.}$	•••	$0.4+0.1E_{c.m.}$	•••	$0.8+0.35E_{c.m.}$	•••

[a] Reference 31.
[b] Reference 34.
[c] Reference 39.

code using the empirically determined imaginary potentials. For this purpose we have fitted Woods-Saxon potentials to the outer tails of our self-consistently calculated energy curves. The potential parameters obtained in this way are listed in Table I.

$^{12}C+^{12}C$. For this system measurements have been available for quite some time.[30-32] The excitation function can satisfactorily be described by the parameters also given in Table I.

The real part of $-V$ is shown in Fig. 8 as a function of the distance r. The dashed curve gives our self-consistently calculated potential. One recognizes quite good agreement whereas a potential based on a surface-energy related folding prescription proposed by Krappe and Nix[33] (KN) has a significantly different slope in the outer region of the interaction.

The calculated barrier radius is somewhat larger than the experimental one and correspondingly is the barrier height of the experimental potential some hundred keV higher than that of our CHF po-

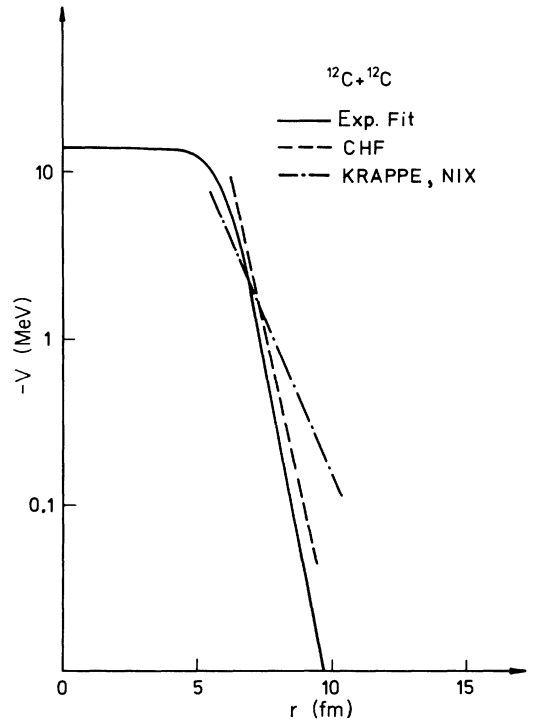

FIG. 8. Comparison of the real part of the optical potential for $^{12}C+^{12}C$. The full line represents an experimental fit. The dashed curve shows the result of our CHF calculations. The dashed-dotted line was calculated according to the Krappe and Nix prescription.

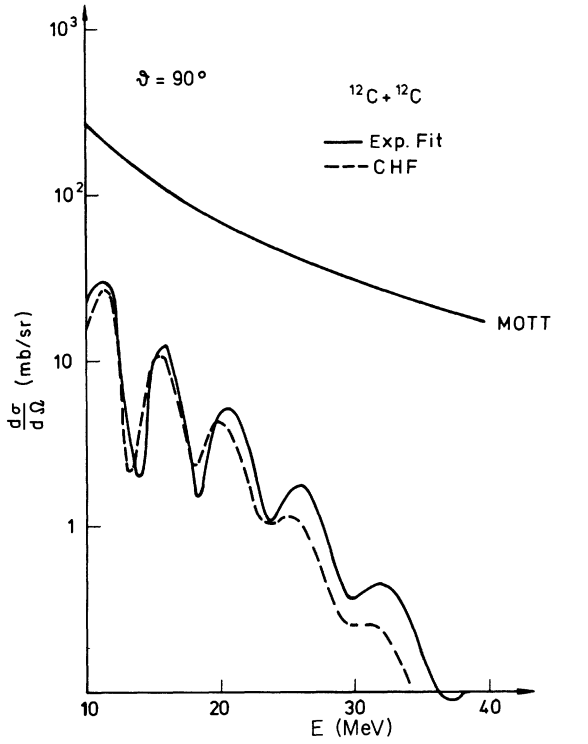

FIG. 9. Excitation functions for the elastic scattering of $^{12}C+^{12}C$. The Mott cross section is represented by the upper full line. The prediction of our CHF calculations (dashed line) is compared with an experimental fit to the data (full line).

tential. The KN potential does not reproduce the experimental curve nearly as well.

Figure 9 shows a typical excitation function at a scattering angle of 90° in the center-of-mass system. In the energy region between 10 and 40 MeV the elastic cross section is much smaller than the Mott cross section due to the absorption. The curves are the results of using the potential of Fig. 8 in an optical model code. In both cases we have used the same imaginary part which was fitted to reproduce the scattering data[31] without further readjustment of its parameters. The position of maxima and minima in the excitation function is in good agreement both with the experimental points and the best fit result. The main remaining differences are the peak to valley ratios and the intermediate structure which cannot be obtained with simple Woods-Saxon type potentials.

$^{16}O+^{16}O$. Let us now switch to our results for the $^{16}O+^{16}O$ system and compare with data obtained by Siemssen *et al.*[34] The best fitting parameters obtained by these authors are also given in Table I. In Fig. 10 we compare the real part of their potential with our result. There is a quite good agreement in the region $r \gtrsim 7$ fm. Again one recognizes an obvious failure of the KN potential as far as the slope of the potential is concerned. The difference between CHF and the experimental potential which increases towards smaller r values disappears more or less if the effect of the spurious relative motion energy is taken into account.

If one calculates the corresponding excitation function using the potentials of Fig. 10, one obtains the results of Fig. 11. Above the Coulomb barrier the cross section drops down over several orders of magnitude. As in the case of carbon we obtain a quite satisfactory agreement between experimental and CHF curves, although again one has to keep in mind the discrepancy between measured points and the prediction of the potentials. In particular, the peak to valley ratio has to be improved. A possible way to do this is to use an l-dependent imaginary part.[35]

An interpretation of the intermediate structure in terms of resonances on the second minimum was proposed by Cherdantsev and Vershinin.[28] However, this resonance effect depends strongly on the form factor and the depth of the imaginary potentials which we cannot calculate at present. We have, therefore, not included the second minimum in our calculations.

The influence of the imaginary potential can also be described in somewhat different words: The CHF energy curve represents only the lowest possible configuration and can be identified with the

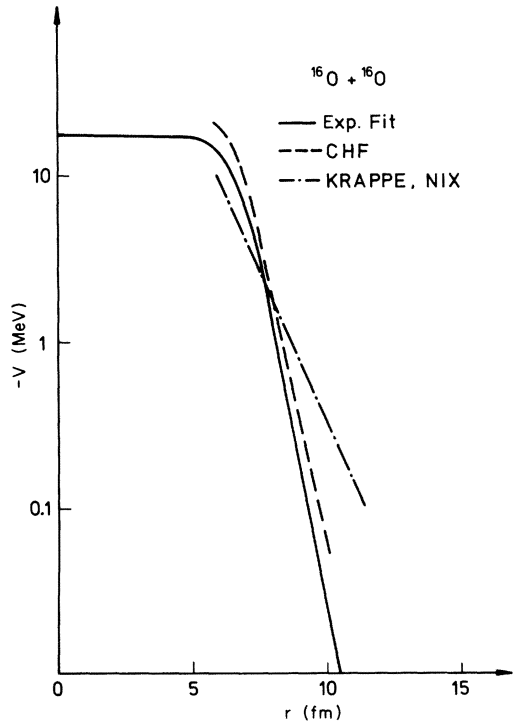

FIG. 10. Real part of the optical potential for $^{16}O+^{16}O$. For an explanation of the various curves see Fig. 8.

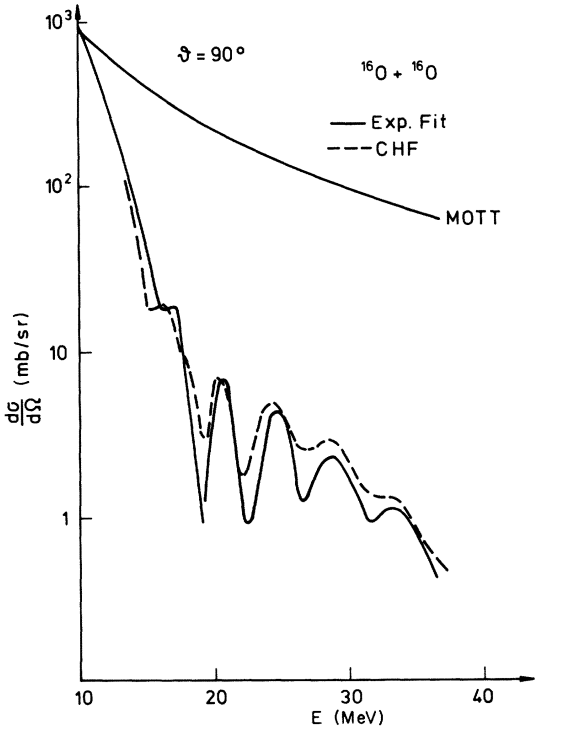

FIG. 11. Excitation functions for the elastic scattering of $^{16}O+^{16}O$.

potential for collective motion only if the coupling between different configurations remains small. In dynamical calculations, however, it was found by Glas and Mosel[36] and Tazawa[37] that for the $^{16}O + ^{16}O$ system the jump probability into higher configurations is very large (of the order of 90%) at the first crossing with a formerly unoccupied state. Since this crossing just leads to the second minimum the existence of this minimum in the *adiabatic* potential curve may be irrelevant for the dynamical evolution of the process.

$^{40}Ca + ^{40}Ca$. For this system experimental data have become available only quite recently. As the two scattering partners are also tightly bound there had been expectations[38] that also in this case the excitation function should exhibit some gross structure. This expectation, however, is not borne out by the data. Instead, the excitation functions obtained by Doubre *et al.*[39] are structureless with a steep downward slope. Therefore, a precise determination of the real part of the potential is difficult.

The parameters obtained by the Orsay group are also given in Table I. Noticeable is the strong imaginary part compared to the $^{16}O + ^{16}O$ case. The physical reason for such a large strength is not yet understood. It should be noted, however, that the strong absorption found by Doube *et al.*[39] is still disputed — at least in the low energy range — in view of the recent contradicting results of the Munich group.[40]

In Fig. 12 we show the real part of the potentials. Our self-consistently calculated potential is nearly identical to the experimental one. There is an excellent agreement for the total interaction potential including the Coulomb term. It is therefore not surprising that we can describe the experimental cross sections very well (Fig. 13). One has, of course, to remember that we always use the imaginary part which is reported by the experimental groups. However, we can conclude that the predictions of CHF calculations for the real part of the optical potential are quite reliable.

V. SUMMARY

It was the aim of the present work to study the applicability of self-consistent methods to the calculation of the real part of HI potentials. The advantage of such a method is threefold: First, it avoids all ambiguities connected with the choice of the nucleon-nucleon interaction by using the same effective force as for the calculation of nuclear ground state properties. The method should thus also have predictive power if applied to very heavy (and eventually also mass-asymmetric) systems. Second, the force used yields very good nuclear

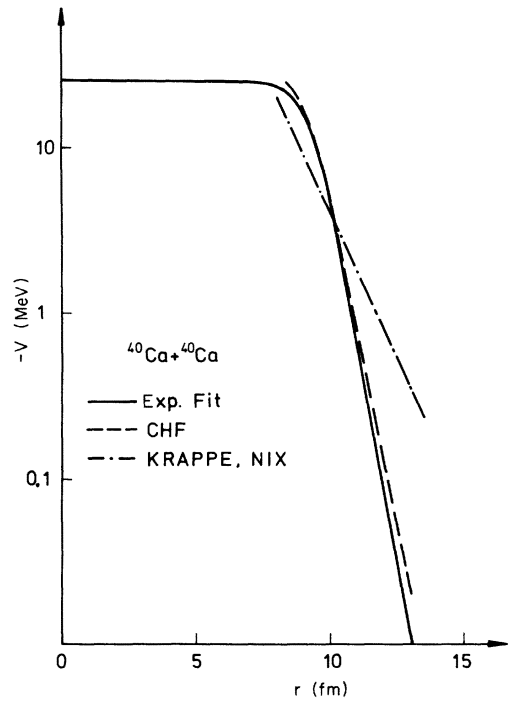

FIG. 12. Real part of the optical potential for the $^{40}Ca + ^{40}Ca$ system.

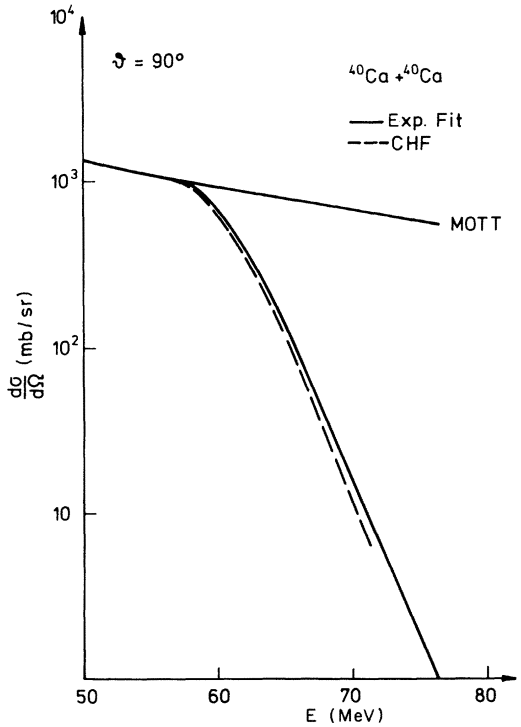

FIG. 13. Excitation functions of the elastic scattering of $^{40}Ca + ^{40}Ca$.

densities as judged from electron scattering. Therefore, the tail regions of the HI that depend critically on the density tails can be calculated quite reliably. Third, the method is free of all *a priori* assumptions on the negligibility of antisymmetrization (AS) effects in the outer potential tails that is tacitly assumed in all folding-model approaches. In contrast, in the CHF method the total wave function of the target-projectile system is completely antisymmetric under exchange of *any* two nucleons at all distances.

The justification for neglecting the AS in the folding method has to our knowledge never been quantitatively investigated. Recent studies of this problem performed by us[18,41,42] have indeed indicated that the AS effects become important as soon as the nuclear potential starts to act and yield a repulsive contribution to the total HI potential (see also Ref. 8). The two less general assumptions of the CHF method are the use of the adiabatic (Born-Oppenheimer) approximation that identifies the total energy of the system at fixed R with the HI potential and the neglect of all possible dynamical effects. The adiabatic approximation should be justified for energies not too far above the barrier so that the collective velocity in R direction remains small. The validity of this method is generally accepted in the literature as shown by e.g., Refs. 3–8. The question of dynamical distortions has been investigated so far only in macroscopic model calculations.[43–45] Here, the question is whether in actual collisions the nuclei "have time" enough to rearrange their shapes such as to attain the lowest possible energy (this, of course, is assumed in a HF procedure). That this requirement may not be met is perhaps indicated by the fact that our CHF potentials all have diffuseness parameters that are too large by 0.07–0.09 fm (see Table I). That the Skyrme force when used in non-self-consistent calculations gives on the contrary a too small diffuseness for the potential[46] points to effects of the self-consistency in our calculations: The nucleons in one nucleus pull the density in the other one over, thus increasing the density diffuseness and correspondingly also that of the potential.

Dynamical distortions can, of course, also be described by a coupling of the adiabatic to other higher lying configurations. The few microscopic calculations available on this point indeed indicate a strong coupling inside a distance corresponding to the sum of the two half-density radii.[36,37]

Besides yielding quite satisfactory HI potentials our calculations have also shown that the shells of the two magic ^{16}O nuclei survive up to a remarkable degree of overlap. Seen from the other side, this means that in the symmetric fission of ^{32}S the shells of the nascent ^{16}O nuclei are felt quite early. This finding may be related to one of the most important conclusions reached in the study of nuclear fission by means of the two-center shell model, namely that the fragment shells have a decisive influence on the potential energy surface for fission.[47,48]

---

*Work supported by Gesellschaft für Schwerionenforschung (GSI) and the Bundesministerium für Forschung und Technologie (BMFT).

[1]C. Toepffer, *Lecture Notes in Physics* (Springer, New York, 1975), Vol. 33, p. 15.
[2]G. Helling, W. Scheid, and W. Greiner, Phys. Lett. 36B, 64 (1971).
[3]K. A. Brueckner, J. R. Buchler, and M. M. Kelly, Phys. Rev. 173, 944 (1968).
[4]W. Scheid and W. Greiner, Z. Phys. 226, 364 (1969).
[5]C. Ngo, B. Tamain, M. Beiner, R. J. Lombard, D. Mas, and H. H. Deubler, Nucl. Phys. A240, 353 (1975).
[6]K. Pruess and W. Greiner, Phys. Lett. 33B, 197 (1970).
[7]U. Mosel, T. D. Thomas, and P. Riesenfeldt, Phys. Lett. 33B, 565 (1970).
[8]D. M. Brink and F. Stancu, Nucl. Phys. A243, 175 (1975).
[9]T. Yukawa, Phys. Lett. 38B, 1 (1972).
[10]H. J. Krappe and J. R. Nix, in *Proceedings of the Third IAEA Symposium on the Physics and Chemistry of Fission, Rochester, 1973* (IAEA, Vienna, 1974), p. 159.
[11]D. Baye and G. Reidemeister, Nucl. Phys. A258, 157 (1976).
[12]T. Fliessbach, Z. Phys. 228, 329 (1970); 242, 287 (1971); 247, 117 (1971).
[13]G. H. Göritz and U. Mosel, Z. Phys. A277, 243 (1976).
[14]G. R. Satchler, in *Proceedings of the International Conference on Reactions between Complex Nuclei, Nashville, 1974,* edited by R. L. Robinson *et al*. (North-Holland, Amsterdam/American Elsevier, New York, 1974), Vol. 2, p. 171; G. R. Satchler, in Proceedings of the Symposium on Macroscopic Features of Heavy Ion Collisions, Argonne, 1976 (unpublished), ANL Report No. ANL/PHY-76-2, p. 33.
[15]B. Sinha, Phys. Rep. 20C, 1 (1975).
[16]D. M. Brink and N. Rowley, Nucl. Phys. A219, 79 (1974).
[17]Y. Eisen and B. Day, Argonne National Laboratory Report No. ANL/PHY-76-2, 1976 (unpublished), p. 541.
[18]P. G. Zint and U. Mosel, Phys. Lett. 56B, 424 (1975).
[19]D. Vautherin and D. M. Brink, Phys. Rev. C 5, 626 (1972).
[20]H. Flocard, P. Quentin, A. K. Kerman, and D. Vautherin, Nucl. Phys. A203, 443 (1973).
[21]P. G. Zint and U. Mosel, Phys. Lett. 58B, 269 (1975).
[22]P. Holzer, U. Mosel, and W. Greiner, Nucl. Phys. A138, 241 (1969); D. Scharnweber, W. Greiner, and U. Mosel, *ibid.* A164, 257 (1971).
[23]E. T. Whittaker and G. N. Watson, *A Course of Modern*

Analysis (Cambridge, U. P., Cambridge, 1952), p. 348.
[24]D. Vautherin, Phys. Rev. C 7, 296 (1973).
[25]P. G. Zint, Ph.D. thesis, University of Giessen, 1975 (unpublished).
[26]H. Flocard, Phys. Lett. 49B, 129 (1974).
[27]S. J. Krieger and C. Y. Wong, Phys. Rev. Lett. 28, 690 (1972).
[28]G. A. Vershinin and P. A. Cherdantsev, Yad. Fiz. 19, 1019 (1974) [Sov. J. Nucl. Phys. 19, 522 (1974)].
[29]U. Mosel, Particles and Nuclei 3, 297 (1972).
[30]D. A. Bromley, J. A. Kuehner, and E. Almquist, Phys. Rev. 123, 878 (1961).
[31]W. Reilly, R. Wieland, A. Gobbi, M. W. Sachs, J. V. Maher, D. Mingay, R. H. Siemssen, and D. A. Bromley, in *Proceedings of the Fifth International Conference on Nuclear Reactions Induced by Heavy Ions, Heidelberg, Germany*, edited by R. Bock and W. R. Hering (North-Holland, Amsterdam, 1970), p. 95.
[32]A. Gobbi, in Proceedings of the Symposium on Heavy Ion Scattering, Argonne, 1971 [Argonne National Laboratory Report No. ANL-7837 (1971)], p. 63.
[33]H. J. Krappe, *Lecture Notes in Physics* (Springer, New York, 1975), Vol 33, p. 24.
[34]R. H. Siemssen, J. V. Maher, A. Weidinger, and D. A. Bromley, Phys. Rev. Lett. 19, 369 (1967).
[35]R. A. Chatwin, J. S. Eck, D. Robson, and A. Richter, Phys. Rev. C 1, 795 (1970).
[36]D. Glas and U. Mosel, Phys. Lett. 49B, 301 (1974).
[37]T. Tazawa, Prog. Theor. Phys. 51, 1764 (1974).
[38]R. Vandenbosch, in Proceedings of the Symposium on Heavy Ion Scattering, Argonne, 1971 [Argonne National Laboratory Report No. ANL-7837 1971], p. 103; and unpublished work (private communication).
[39]H. Doubre, J. C. Raynett, J. C. Jacmart, N. Poffé, and R. Rion, Phys. Rev. Lett. 35, 508 (1975).
[40]W. Henning, H. J. Körner, R. Müller, K. E. Rehm, M. Richter, H. P. Rother, H. Schaller, and H. Spieler, Verhandl. DPG (VI) 11, 816 (1976).
[41]J. Fleckner, Diploma thesis, University of Giessen, 1976 (unpublished).
[42]U. Mosel, in Proceedings of the Symposium on Macroscopic Features of Heavy Ion Collisions, Argonne National Laboratory, April 1976 (unpublished), Argonne Report No. ANL/PHY-76-2, p. 341.
[43]A. S. Jensen and C. Y. Wong, Nucl. Phys. A171, 1 (1971).
[44]H. Holm and W. Greiner, Nucl. Phys. A195, 333 (1972).
[45]P. W. Riesenfeldt and T. D. Thomas, Phys. Rev. C 2, 711 (1970).
[46]F. Stancu and D. M. Brink, Univ. of Oxford report, 1976 (unpublished).
[47]U. Mosel and H. W. Schmitt, Phys. Rev. C 4, 2185 (1971).
[48]M. G. Mustafa, U. Mosel, and H. W. Schmitt, Phys. Rev. C 7, 1519 (1973).